Ultrastrong Mode Confinement in ZnO Surface Plasmon Nanolasers

Yu-Hsun Chou,[†,‡] Bo-Tsun Chou,[§] Chih-Kai Chiang,[∥] Ying-Yu Lai,[‡] Chun-Ting Yang,[‡] Heng Li,[‡] Tzy-Rong Lin,[∥,⊥] Chien-Chung Lin,[†] Hao-Chung Kuo,[‡] Shing-Chung Wang,[‡] and Tien-Chang Lu*[,‡]

[†]Institute of Lighting and Energy Photonics, National Chiao Tung University, Tainan, Taiwan, [‡]Department of Photonics and [§]Department of Electronics Engineering, National Chiao Tung University, Hsinchu, Taiwan, and [∥]Institute of Optoelectronic Sciences and [⊥]Department of Mechanical and Mechatronic Engineering, National Taiwan Ocean University, Keelung, Taiwan

ABSTRACT Nanolasers with an ultracompact footprint can provide high-intensity coherent light, which can be potentially applied to high-capacity signal processing, biosensing, and subwavelength imaging. Among various nanolasers, those with cavities surrounded by metals have been shown to have superior light emission properties because of the surface plasmon effect that provides enhanced field confinement capability and enables exotic light–matter interaction. In this study, we demonstrated a robust ultraviolet ZnO nanolaser that can operate at room temperature by using silver to dramatically shrink the mode volume. The nanolaser shows several distinct features including an extremely small mode volume, a large Purcell factor, and a slow group velocity, which ensures strong interaction with the exciton in the nanowire.

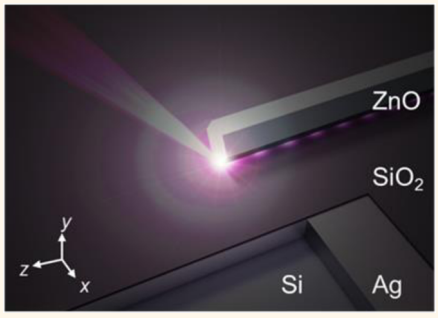

KEYWORDS: nanolaser · surface plasmon · ZnO · nanowire · silver

The quest for small coherent light sources has never been stopped, as these micro- to nanoscale light sources not only are essential for small-footprint, low power consumption, high-density, and parallel signal processing applications[1−11] but also provide an insightful way to investigate the interaction between light and matter.[5−7,9,10,12−15] Several designs have been developed to scale down the optical cavity volume to contain only a few photon modes, such as photonic crystal defect type lasers,[2,16] microdisk lasers,[17] and nanowire lasers.[1,11] These lasers, however, require a cavity size on the order of a few $(\lambda/n)^3$ to sustain a proper mode profile with a reasonable cavity Q value. Recently, optical cavities surrounded by metal claddings have been developed to reduce the cavity volume because the optical field penetrating into the metal claddings decays so rapidly that the optical mode can be further shrunk at the cost of a lower cavity Q value because of the strong absorption of the metal.[3,8,18] However, the metal can provide a method for drastically diminishing the cavity mode beyond the diffraction limit by forming a surface plasmon at the interface of the metal and dielectric layers.[19] The ultrasmall electromagnetic field distribution of the surface plasmon mode can substantially facilitate the interaction between light and matter by enhancing the Purcell factor.[20−22] Furthermore, a novel type of surface plasmon-based amplification of stimulated emission of radiation (spaser) has been proposed[15] and demonstrated.[5] A group of Au nanospheres[5] and Au nanorods[23] coated with a gain medium and a two-dimensional array of protruding Au bowtie nanostructures[14] sitting on the active medium facilitates the spasing action based particularly on the localized surface plasmon mode. Additionally, an unambiguous demonstration of a single nanolaser has been performed using the nanowire gain medium lying on the metal separated by a thin dielectric layer to form a Fabry–Perot-type surface plasmon (or surface plasmon polariton) cavity.[6,10] Because the emitted photons have one-to-one corresponding characteristics to the cavity surface plasmons, these photons also show a coherent signature. A higher cavity Q value can be realized using a nanosquare to form a whispering gallery surface plasmon mode facilitated by the total internal reflection.[7] With the improvement of a cavity Q value, nanolaser operation can be performed at room temperature.

* Address correspondence to timtclu@mail.nctu.edu.tw.

Received for review December 28, 2014 and accepted April 8, 2015.

Published online April 08, 2015
10.1021/acsnano.5b01643

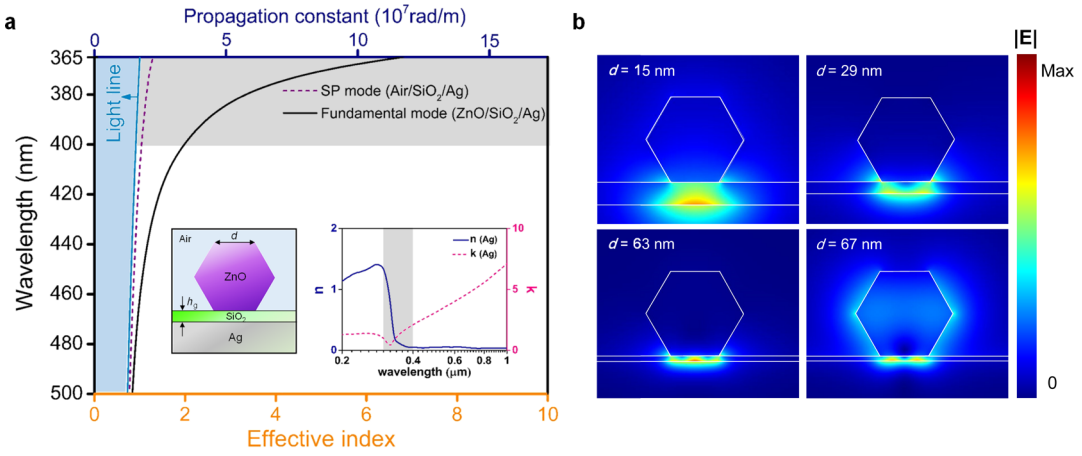

Figure 1. Dispersion curves and mode profiles of a ZnO nanowire with a hexagonal cross section. (a) The inset to the left shows the schematic cross section of a ZnO nanolaser. The side length (d) of the hexagon and the thickness (h_g) of the SiO_2 spacer are 28 and 7 nm, respectively. The azure blue solid line represents the light line, and the purple dashed line represents the surface plasmon mode dispersion when only considering the air−SiO_2−Ag slab. The black solid line shows the fundamental surface plasmon (F) mode dispersion in the ZnO nanolaser structure on the SiO_2−Ag slab. The rapid increase of the effective index in the gray-shaded wavelength range for the Ag case is due to the background polarization of Ag provided by the interband absorption, which can be observed in the gray-shaded area, shown in the inset to the right. (b) When d is smaller than 29 nm, only surface plasmon F mode can exist, as shown in the upper left mode profile. The surface plasmon first and second modes appear when d is larger than 29 and 63 nm, as shown in the upper right and lower left mode profiles, respectively. The dielectric-like mode can appear only when d is larger than 67 nm, as shown in the lower right mode profile.

The successful demonstration of a plasmon nanolaser typically relies on its enhanced Purcell factor, which is inversely proportional to the mode volume. In addition, the slower propagating speed of plasmons can raise the Purcell factor by increasing opportunities for interaction between the gain medium and surface plasmons. Slow group velocity can be achieved at the band edge provided by the distributed feedback mechanism in the two-dimensional periodic structure.[12,13] However, the distributed feedback mechanism requires a relatively large area, which violates the small dimension requirement of nanolasers. The refractive index of silver (Ag) exhibits high variation in the ultraviolet (UV) wavelength range because of the interband absorption,[24] as shown in the inset on the right in Figure 1a. This index variation can directly influence the dispersion of the surface plasmon to achieve a large group index, resulting in a small mode volume and large Purcell factor. To demonstrate this effect, we used a zinc oxide (ZnO) nanowire as the gain medium to match the UV wavelength range. The large exciton binding energy and oscillator strength of ZnO are also beneficial to the coupling between the ZnO exciton and surface plasmon. In this study, we reported the UV nanolaser operation based on the exciton−surface-plasmon coupling at room temperature. A large group index and small mode volume, accompanied by an enhanced Purcell factor, a reasonable Q value, and a large confinement factor, ensured that our ZnO surface plasmon nanolasers were operated below the exciton Mott density and at room temperature. Such UV plasmon nanolasers have numerous potential applications such as in biosensing,[25] optical storage,[26] subwavelength imaging, and photolithography.[27]

RESULTS AND DISCUSSION

Figure 1a shows the dispersion curves of fundamental surface plasmon modes for the ZnO nanocavity calculated by a finite-element method from the commercial package Comsol Multiphysics,[28] in which the refractive indices of metals and ZnO were taken from previous studies.[29,30] The side length of the cross-sectional ZnO hexagon and the thickness of the SiO_2 film were 28 and 7 nm, respectively. The effective indices of fundamental surface plasmon modes increased rapidly as the wavelength entered the UV band within the gray-shaded area as shown in Figure 1a. The surface plasmon could be confined at a wavelength of 373 nm for the fundamental mode. The effective mode volume for the fundamental surface plasmon mode is calculated as $4.2 \times 10^{-3}\lambda^3$ with a group index of 79 (Supporting Information section 1.2). The effective mode volume (V_m) of our ZnO plasmonic nanolaser is defined as

$$V_m = \frac{W_m}{\max[W(r)]} = \frac{\iiint W(r)\, d^3r}{\max[W(r)]}$$

where W_m is the total mode energy, $W(r)$ is the mode energy density, and $\max[W(r)]$ is the maximum energy density. Our plasmonic nanolaser is operated in the UV regime, in which the Ag-based plasmonic cavity has a strong material dispersion behavior; therefore, to acquire precise simulation results, the material dispersive properties of Ag and ZnO nanowires were taken into account during the simulation. The mode energy density is defined as follows:

$$W(r) = \frac{1}{2}\left[\mathrm{Re}\left[\frac{d(\omega\varepsilon)}{d\omega}\right]|E(r)|^2 + \mu|H(r)|^2\right]$$

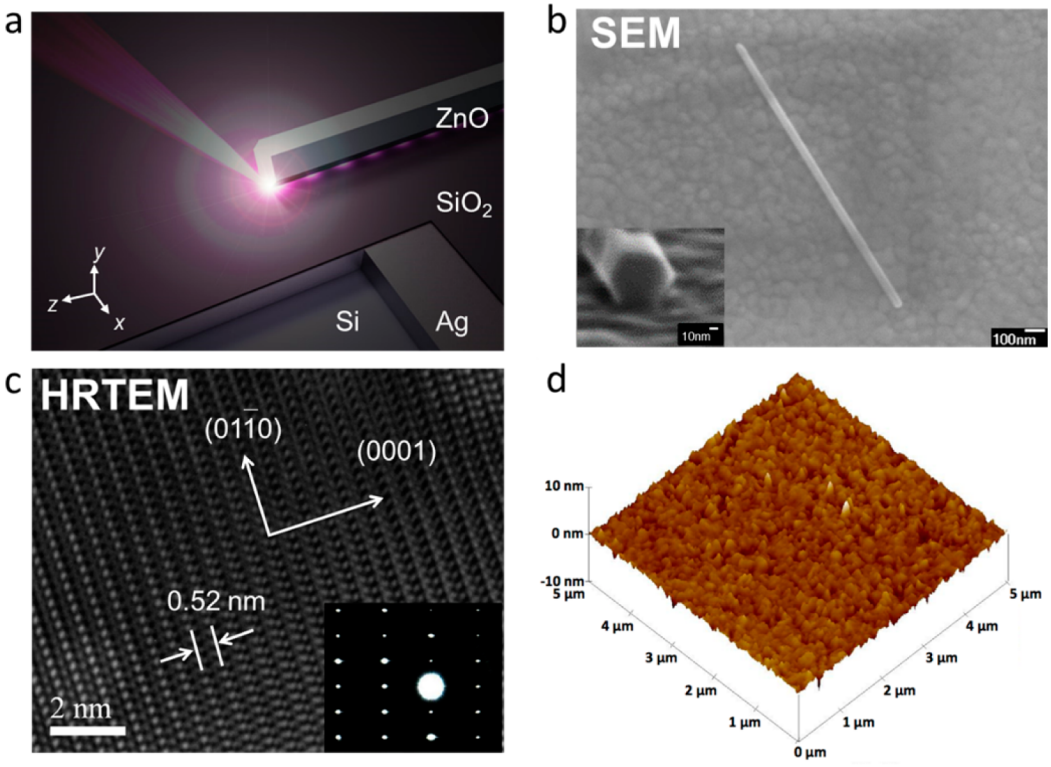

Figure 2. Structure and crystalline characterization of the ZnO surface plasmon nanolaser. (a) Schematic bird's eye view diagram of a ZnO nanowire lying on top of the high-quality Ag film with a thin SiO_2 spacer layer. (b) Scanning electron microscope image of the ZnO nanolaser device. The inset figure is the cross-sectional view of a ZnO nanowire. (c) High-resolution transmission electron microscopy (HRTEM) image of a ZnO nanowire taken from the [2$\bar{1}\bar{1}$0] direction. The lattice fringe spacing in the HRTEM image is 0.52 nm, which corresponds to the lattice constant of the hexagonal wurtzite structure of ZnO and indicates that the nanowire's growth is along the [0001] direction. (d) 5 μm $\times$ 5 μm AFM images of the 7 nm thick SiO_2 grown on single-crystalline Ag film.

where ε is the permittivity and μ is the permeability. The effective mode volume is 1 order of magnitude smaller compared with previously reported surface plasmon nanowire lasers[6,10,31,32] mainly because of the close contact between the hexagonal side and the metal and the lower effective plasmon frequency of Ag modulated by the interband absorption at the UV band. Because the side length of the ZnO hexagon was smaller than 67 nm, only the surface plasmon modes could exist in the nanocavity, as shown in Figure 1b.

Figure 2a shows a bird's eye view of the schematic semiconductor−insulator−metal (SIM) structure, including a ZnO nanowire on a high-quality Ag thin film[33] with a thin SiO_2 spacer layer. Figure 2b shows the top view of a ZnO nanowire on the Ag film, and the inset shows the end facet with a hexagonal shape. The typical side length of the ZnO nanowires ranges from 25 to 50 nm, the length of the ZnO nanowires ranges from approximately 1 to 2 μm, and the growing direction is the *c*-axis of the wurtzite structure (Figure 2c). A single ZnO nanowire with a length of 1.24 μm on a Ag film with a 7 nm thick SiO_2 spacer was pumped at 77 K with a pumping laser wavelength of 355 nm. The measured emission spectra at different pumping densities are shown in Figure 3a. Broad spontaneous emission spectra were observed until the threshold at 60 MW/cm^2 was achieved with an obvious line width narrowing to 0.4 nm, as shown in the inset of Figure 3a, demonstrating a clear lasing transition. A well-known two-slope light−light curve for the lasing peak can be obtained, as shown in the inset of Figure 3a. The light−light curve was fitted by using modified rate equations (Supporting Information section 4), and the spontaneous emission factor was determined to be 0.5. At a higher pumping density, multiple lasing peaks appear and dominate the spectra. These multiple lasing peaks are the signature of longitudinal modes along the nanowire. We measured the degree of polarization for three strong lasing modes and found that they were highly polarized along the nanowire direction, as shown in the inset of Figure 3a. The consistent polarization direction ensures that these longitudinal lasing modes all belong to the fundamental surface plasmon mode (Supporting Information section 1.3). Furthermore, a small mode spacing value ($\Delta\lambda \approx 0.7$ nm) resulted in a large group index of approximately 80, as shown in Figure 3b,c, which is consistent with our calculation. The large group index in our nanowire cavity resulted from the highly dispersive surface plasmon mode, which not only caused an extremely small mode volume that enlarged the Purcell factor but also equipped the

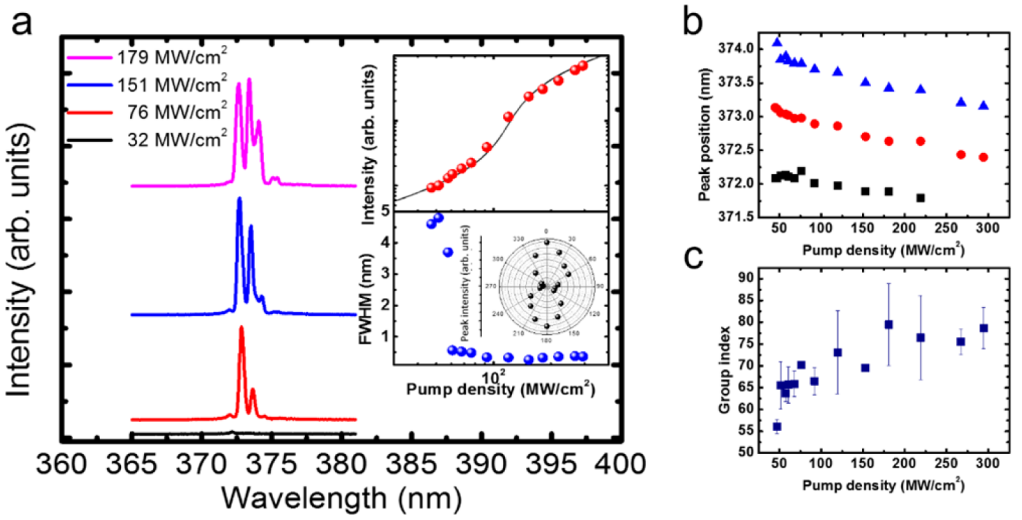

Figure 3. Lasing characteristics of a ZnO surface plasmon nanolaser at 77 K. The physical dimensions of the measured device are as follows: the length of the nanowire is 1.24 μm; the side length of the cross-sectional hexagon is 28 nm; and the thickness of the spacer is 7 nm. (a) Measured spectra at the laser pumping power density from 32 to 179 MW/cm^2. The solid red sphere line in the inset is the light−light curve of the emission peak at 373 nm. The black solid line is the fitted curve calculated using the modified rate equations. The solid blue sphere line in the inset shows the line width of the emission peak *versus* the pumping power density. The solid black sphere line in the inset shows the corresponding polar plot of the emission intensity. The polarization direction of the lasing modes is along the nanowire length with a degree of polarization of 52%. (b) Peak positions extracted from the emission spectra in (a) at the laser pumping power density from 32 to 300 MW/cm^2. (c) The group index above the threshold is calculated using $n_g = \lambda^2/2\Delta\lambda L$, where $\Delta\lambda$ is extracted from (b) and L is the length of the nanowire.

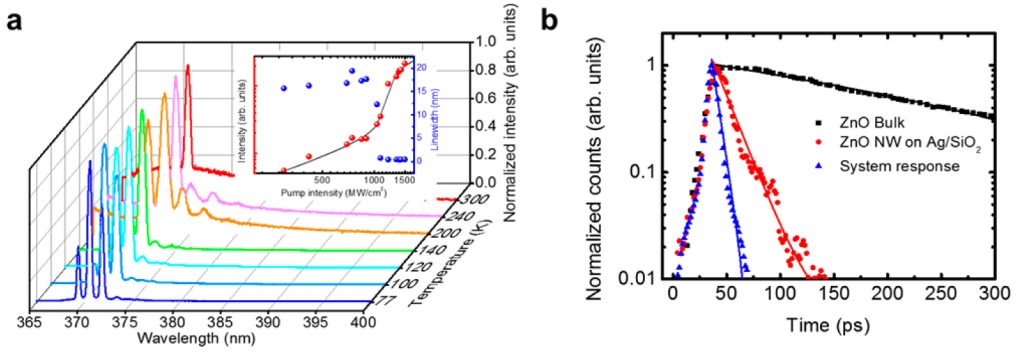

Figure 4. Temperature-dependent lasing spectra and time-resolved PL signals of the ZnO surface plasmon nanolaser. (a) Emission spectra measured at temperatures from 77 to 300 K with a pumping power density of 1262 MW/cm^2. The length of the ZnO nanowire is 1.73 μm. Distinct lasing spectra with narrow lasing line widths were observed at temperatures from 77 to 300 K. The details of the mode spacing affected by temperature are discussed in Supporting Information section 3. Inset: Solid red and blue sphere lines are the light−light curve and line width of the emission peak at 300 K, and the black solid line is the fitted curve calculated using the modified rate equations. (b) Time-resolved PL signals (dots) and fitted curves (solid lines) at 77 K show a decay time of 265 ps for ZnO bulk (black square dots and line), a decay time of 13 ps (red circle dots and line) for a ZnO nanowire lying on a Ag film with a 7 nm thick SiO_2 spacer, and a system response of 6.4 ps (blue triangular dots and line). The time-resolved spectra were recorded at an excitation power of 12 mW.

surface plasmon with higher momentum to interact with the ZnO exciton. The strong interaction between the exciton and surface plasmon is evidenced by the obvious blue-shift tendency of the lasing peaks above the threshold, as shown in Figure 3b. Unlike the ordinary photon laser, the blue-shifted peak above the threshold has been commonly observed in strongly coupled microcavity exciton-polariton lasers[34,35] and the nanocavity spasers.[7,10] In this study, we developed a novel class of hybridized coherence states through coupling the exciton and surface plasmon.

To test the robustness of our ZnO plasmon nanolaser, we increased the operation temperature from 77 K to room temperature. The temperature-dependent emission spectra are shown in Figure 4a. The inset of Figure 4a shows 300 K experimental results for the line width variation and light−light curve fitted using modified rate equations with a spontaneous emission factor of 0.15. The lasing action can be sustained up to 300 K, outperforming previous plasmonic Fabry−Perot-type nanolasers.[6,10] This is because of the well-confined mode profile and high momentum of the surface plasmon that efficiently couples to the ZnO exciton, in which the large exciton binding energy of ZnO can provide enough excitonic gain to overcome the loss of the nanocavity at room temperature.

We believe that the refined nanocavity geometry and fabrication process can allow the ZnO plasmon laser to be operated at a higher temperature. In terms of carrier dynamics, the ZnO exciton originally had high oscillator strength, corresponding to a relatively fast exciton decay. The exciton decay time of ZnO bulk at 77 K was measured to be 265 ps by using the streak camera detection, as shown in Figure 4b. However, the exciton decay time of a ZnO nanowire on an Ag film with a 7 nm thick SiO_2 spacer was further reduced to 13 ps, corresponding to an average Purcell factor of 20.4. Although the Purcell factor and group velocity are linked quantities, the difference between these values in our experiment was caused by homogeneous, inhomogeneous broadening[36] and the average lifetime collected by the entire nanowire. This large Purcell factor originated from the tightly confined surface plasmon mode, which strongly interacted with the exciton. This manifests not only a robust laser operation up to room temperature but also the extremely fast energy transfer between excitons and surface plasmons, implying that an ultrafast modulation speed can be expected.[32]

CONCLUSIONS

We demonstrated a room-temperature UV ZnO surface plasmon nanolaser with an effective mode volume 1000 times smaller than the cubic vacuum wavelength, which is by far the smallest single coherent light source reported. By utilizing the large dispersive surface plasmon characteristics in Ag, we can further shrink the surface plasmon mode volume to efficiently enhance the Purcell factor and simultaneously raise the momentum of the surface plasmon to strongly interact with the ZnO exciton. The measured average Purcell factor can be larger than 20, and the group velocity of the surface plasmon can be reduced to 1/80 of the speed of light. Our demonstration of a UV nanolaser operated at room temperature can be applied to biosensing, subwavelength imaging, and nanoscale photolithography. Moreover, the ultrafast and strong interaction between surface plasmons and excitons provides a new class of coherent sources for the quantum plasmonic test bed.

METHODS

The UV ZnO surface plasmon nanolasers were developed by placing ZnO nanowires on a high-quality Ag film with a thin SiO_2 spacer layer based on the SIM structure[6,10] (inset on the left in Figure 1a), in which the thin SiO_2 spacer greatly reduced the metal loss. The lateral nanocavity dimension was defined by the nanowire length and one side of the hexagon. We used the electron-gun evaporator to deposit a 200 nm thick Ag thin film on the (100) intrinsic silicon substrate and then annealed the Ag film at 340 °C. The root-mean-square roughness of the Ag film was approximately 0.5 nm (Supporting Information section 5.1), followed by the SiO_2 layer evaporated on the Ag film. Metal patterned squares of 10 μm by 10 μm were produced on the SiO_2 layer to identify the exact position of a single ZnO nanowire. The single-crystalline ZnO nanowires were fabricated using a hydrothermal method in powder form.[37] We then dispersed ZnO nanowire powders with an isopropyl alcohol (IPA) solution and drop-casted the solution on the patterned substrate. After the evaporation of the IPA solution, ZnO nanowires were then attached to the patterned SiO_2/Ag substrate. To confirm that the optical signals were emitted from a single ZnO nanowire with no other nanowires nearby, we used a scanning electron microscope and a charge-coupled device (CCD) camera to search for the locations of the patterned squares with only a single ZnO nanowire. The ZnO nanowire was then optically pumped using a third-harmonic generation of a Nd:YVO_4 355 nm pulse laser with a 0.5 ns pulse duration and a 1 kHz repetition rate. By using a 100× near-UV infinity-corrected objective lens with a numerical aperture (NA) of 0.55 (Mitutoyo), the pumping beam was normally incident onto the patterned square and the diameter of the pumping beam was 15 μm. The reflected light was collected using a 600 μm core UV optical fiber and detected using a CCD attached to a 320 mm single monochromator (HR320, Jobin-Yvon) with a spectral resolution of approximately 0.2 nm. Two emission spots from the end points of a ZnO nanowire were observed using the CCD camera (Supporting Information section 6.1). A polarizer was placed in front of the fiber to measure the degree of polarization, defined by $(I_{max} - I_{min})/(I_{max} + I_{min})$ where I_{max} and I_{min} are the maximum and the minimum intensities of the lasing peak. For time-resolved PL experiments, a 266 nm laser pulse was generated by tripling the frequency of a Ti:sapphire laser (Mira 900, Coherent) with a 76 MHz repetition rate, and a 200 fs pulse duration was used as the probe beam. The PL signal emitted from the sample was collected using a 50× plane UV infinity-corrected objective lens and fed into a streak camera (Hamamtsu, C5680) with a temporal resolution of approximately 6 ps in the single-shot mode.

Conflict of Interest: The authors declare no competing financial interest.

Acknowledgment. The authors acknowledge the help of Tsu-Chi Chang, Bo-Hao Huang, and Pi-Ju Cheng at National Chiao Tung University and Yi-Chen Chung and Chien-Wei Wu at National Taiwan Ocean University for technical support. This work was partially supported by the Ministry of Education Aim for the Top University Program and by the Minister of Science and Technology (MOST) under Contract Nos. NSC100-2628-E009-013-MY3 and NSC102-2221-E-019-050.

Supporting Information Available: Details of surface plasmon mode simulation, optical characteristics of ZnO nanowires lying on different substrates, temperature effects, rate equation analysis, and fabrication process, as well as the optical measurement setup. This material is available free of charge *via* the Internet at http://pubs.acs.org.

REFERENCES AND NOTES

1. Huang, M. H.; Mao, S.; Feick, H.; Yan, H. Q.; Wu, Y. Y.; Kind, H.; Weber, E.; Russo, R.; Yang, P. D. Room-Temperature Ultraviolet Nanowire Nanolasers. *Science* **2001**, *292*, 1897–1899.
2. Noda, S. Seeking the Ultimate Nanolaser. *Science* **2006**, *314*, 260–261.
3. Hill, M. T.; Oei, Y. S.; Smalbrugge, B.; Zhu, Y.; De Vries, T.; Van Veldhoven, P. J.; Van Otten, F. W. M.; Eijkemans, T. J.; Turkiewicz, J. P.; De Waardt, H.; *et al*. Lasing in Metallic-Coated Nanocavities. *Nat. Photonics* **2007**, *1*, 589–594.
4. Zimmler, M. A.; Bao, J.; Capasso, F.; Muller, S.; Ronning, C. Laser Action in Nanowires: Observation of the Transition from Amplified Spontaneous Emission to Laser Oscillation. *Appl. Phys. Lett.* **2008**, *93*, 051101.

5. Noginov, M. A.; Zhu, G.; Belgrave, A. M.; Bakker, R.; Shalaev, V. M.; Narimanov, E. E.; Stout, S.; Herz, E.; Suteewong, T.; Wiesner, U. Demonstration of a Spaser-Based Nanolaser. *Nature* **2009**, *460*, 1110–U68.
6. Oulton, R. F.; Sorger, V. J.; Zentgraf, T.; Ma, R. M.; Gladden, C.; Dai, L.; Bartal, G.; Zhang, X. Plasmon Lasers at Deep Subwavelength Scale. *Nature* **2009**, *461*, 629–632.
7. Ma, R. M.; Oulton, R. F.; Sorger, V. J.; Bartal, G.; Zhang, X. A. Room-Temperature Sub-Diffraction-Limited Plasmon Laser by Total Internal Reflection. *Nat. Mater.* **2011**, *10*, 110–113.
8. Ding, K.; Ning, C. Z. Metallic Subwavelength-Cavity Semiconductor Nanolasers. *Light-Sci. Appl.* **2012**, *1*, e20.
9. Khajavikhan, M.; Simic, A.; Katz, M.; Lee, J. H.; Slutsky, B.; Mizrahi, A.; Lomakin, V.; Fainman, Y. Thresholdless Nanoscale Coaxial Lasers. *Nature* **2012**, *482*, 204–207.
10. Lu, Y. J.; Kim, J.; Chen, H. Y.; Wu, C. H.; Dabidian, N.; Sanders, C. E.; Wang, C. Y.; Lu, M. Y.; Li, B. H.; Qiu, X. G.; *et al*. Plasmonic Nanolaser Using Epitaxially Grown Silver Film. *Science* **2012**, *337*, 450–453.
11. Saxena, D.; Mokkapati, S.; Parkinson, P.; Jiang, N.; Gao, Q.; Tan, H. H.; Jagadish, C. Optically Pumped Room-Temperature Gaas Nanowire Lasers. *Nat. Photonics* **2013**, *7*, 963–968.
12. Zhou, W.; Dridi, M.; Suh, J. Y.; Kim, C. H.; Co, D. T.; Wasielewski, M. R.; Schatz, G. C.; Odom, T. W. Lasing Action in Strongly Coupled Plasmonic Nanocavity Arrays. *Nat. Nanotechnol.* **2013**, *8*, 506–511.
13. van Beijnum, F.; van Veldhoven, P. J.; Geluk, E. J.; de Dood, M. J. A.; 't Hooft, G. W.; van Exter, M. P. Surface Plasmon Lasing Observed in Metal Hole Arrays. *Phys. Rev. Lett.* **2013**, *110*, 206802.
14. Suh, J. Y.; Kim, C. H.; Zhou, W.; Huntington, M. D.; Co, D. T.; Wasielewski, M. R.; Odom, T. W. Plasmonic Bowtie Nanolaser Arrays. *Nano Lett.* **2012**, *12*, 5769–5774.
15. Bergman, D. J.; Stockman, M. I. Surface Plasmon Amplification by Stimulated Emission of Radiation: Quantum Generation of Coherent Surface Plasmons in Nanosystems. *Phys. Rev. Lett.* **2003**, *90*, 027402.
16. Takeda, K.; Sato, T.; Shinya, A.; Nozaki, K.; Kobayashi, W.; Taniyama, H.; Notomi, M.; Hasebe, K.; Kakitsuka, T.; Matsuo, S. Few-Fj/Bit Data Transmissions Using Directly Modulated Lambda-Scale Embedded Active Region Photonic-Crystal Lasers. *Nat. Photonics* **2013**, *7*, 569–575.
17. Tamboli, A. C.; Haberer, E. D.; Sharma, R.; Lee, K. H.; Nakamura, S.; Hu, E. L. Room-Temperature Continuous-Wave Lasing in Gan/Ingan Microdisks. *Nat. Photonics* **2007**, *1*, 61–64.
18. Nezhad, M. P.; Simic, A.; Bondarenko, O.; Slutsky, B.; Mizrahi, A.; Feng, L. A.; Lomakin, V.; Fainman, Y. Room-Temperature Subwavelength Metallo-Dielectric Lasers. *Nat. Photonics* **2010**, *4*, 395–399.
19. Barnes, W. L.; Dereux, A.; Ebbesen, T. W. Surface Plasmon Subwavelength Optics. *Nature* **2003**, *424*, 824–830.
20. Andersen, M. L.; Stobbe, S.; Sorensen, A. S.; Lodahl, P. Strongly Modified Plasmon-Matter Interaction with Mesoscopic Quantum Emitters. *Nat. Phys.* **2011**, *7*, 215–218.
21. Tame, M. S.; McEnery, K. R.; Ozdemir, S. K.; Lee, J.; Maier, S. A.; Kim, M. S. Quantum Plasmonics. *Nat. Phys.* **2013**, *9*, 329–340.
22. de Leon, N. P.; Lukin, M. D.; Park, H. Quantum Plasmonic Circuits. *IEEE J. Sel. Top. Quant. Electron.* **2012**, *18*, 1781–1791.
23. Meng, X. G.; Kildishev, A. V.; Fujita, K.; Tanaka, K.; Shalaev, V. M. Wavelength-Tunable Spasing in the Visible. *Nano Lett.* **2013**, *13*, 4106–4112.
24. Ehrenreich, H.; Philipp, H. R. Optical Properties of Ag and Cu. *Phys. Rev.* **1962**, *128*, 1622–1629.
25. Anker, J. N.; Hall, W. P.; Lyandres, O.; Shah, N. C.; Zhao, J.; Van Duyne, R. P. Biosensing with Plasmonic Nanosensors. *Nat. Mater.* **2008**, *7*, 442–453.
26. Zijlstra, P.; Chon, J. W. M.; Gu, M. Five-Dimensional Optical Recording Mediated by Surface Plasmons in Gold Nanorods. *Nature* **2009**, *459*, 410–413.
27. Schuller, J. A.; Barnard, E. S.; Cai, W. S.; Jun, Y. C.; White, J. S.; Brongersma, M. L. Plasmonics for Extreme Light Concentration and Manipulation. *Nat. Mater.* **2010**, *9*, 193–204.
28. *Comsol Multiphysics*; COMSOL Inc.: Burlington, MA, Comsol 4.4, 2014.
29. Johnson, P. B.; Christy, R. W. Optical Constants of the Noble Metals. *Phys. Rev. B* **1972**, *6*, 4370–4379.
30. Ozgur, U.; Alivov, Y. I.; Liu, C.; Teke, A.; Reshchikov, M. A.; Dogan, S.; Avrutin, V.; Cho, S. J.; Morkoc, H. A Comprehensive Review of ZnO Materials and Devices. *J. Appl. Phys.* **2005**, *98*, 041301.
31. Zhang, Q.; Li, G. Y.; Liu, X. F.; Qian, F.; Li, Y.; Sum, T. C.; Lieber, C. M.; Xiong, Q. H. A Room Temperature Low-Threshold Ultraviolet Plasmonic Nanolaser. *Nat. Commun.* **2014**, *5*, 4953.
32. Sidiropoulos, T. P. H.; Roder, R.; Geburt, S.; Hess, O.; Maier, S. A.; Ronning, C.; Oulton, R. F. Ultrafast Plasmonic Nanowire Lasers near the Surface Plasmon Frequency. *Nat. Phys.* **2014**, *10*, 870–876.
33. Chou, B. T.; Huang, B. H.; Lu, T. C.; Lin, S. D. Single-Crystalline Silver Film Grown on Si (100) Substrate by Using Electron-Gun Evaporation and Thermal Treatment. *J. Vac. Sci. Technol. B* **2014**, *32*, 031209.
34. Deng, H.; Weihs, G.; Snoke, D.; Bloch, J.; Yamamoto, Y. Polariton Lasing vs. Photon Lasing in a Semiconductor Microcavity. *Proc. Natl. Acad. Sci. U.S.A.* **2003**, *100*, 15318–15323.
35. Chen, J. R.; Lu, T. C.; Wu, Y. C.; Lin, S. C.; Hsieh, W. F.; Wang, S. C.; Deng, H. Characteristics of Exciton-Polaritons in ZnO-Based Hybrid Microcavities. *Opt. Express* **2011**, *19*, 4101–4112.
36. Gu, Q.; Slutsky, B.; Vallini, F.; Smalley, J. S. T.; Nezhad, M. P.; Frateschi, N. C.; Fainman, Y. Purcell Effect in Sub-Wavelength Semiconductor Lasers. *Opt. Express* **2013**, *21*, 15603–15617.
37. Baruah, S.; Dutta, J. Hydrothermal Growth of Zno Nanostructures. *Sci. Technol. Adv. Mater.* **2009**, *10*, 013001.